Sensors and Actuators A 158 (2010) 183–192

Contents lists available at ScienceDirect

Sensors and Actuators A: Physical

journal homepage: www.elsevier.com/locate/sna

Development of piezoelectric acoustic sensor with frequency selectivity for artificial cochlea

Hirofumi Shintaku [a,*], Takayuki Nakagawa [b], Dai Kitagawa [a], Harto Tanujaya [a], Satoyuki Kawano [a], Juichi Ito [b]

[a] *Department of Mechanical Science and Bioengineering, Graduate School of Engineering Science, Osaka University, Machikaneyama-cho 1-3, Toyonaka, Osaka 560-8531, Japan*

[b] *Department of Otolaryngology, Head and Neck Surgery, Graduate School of Medicine, Kyoto University, Kawahara-cho 54,Shogoin, Sakyo-ku, Kyoto 606-8507, Japan*

ARTICLE INFO

Article history:
Received 25 July 2009
Received in revised form
13 November 2009
Accepted 22 December 2009
Available online 4 January 2010

Keywords:
Fluid-structure interaction
Acoustic MEMS sensor
Artificial cochlea
Biomechanical engineering
Piezoelectric device

ABSTRACT

In this paper, we report a novel piezoelectric artificial cochlea which realizes both acoustic/electric conversion and frequency selectivity without an external energy supply. The device comprises an artificial basilar membrane (ABM) which is made of a 40 μm thick polyvinylidine difluoride (PVDF) membrane fixed on a substrate with a trapezoidal slit. The ABM over the slit, which mimics the biological system, is vibrated by acoustic waves and generates electric output due to the piezoelectric effect of PVDF. The width of ABM is linearly varied from 2.0 to 4.0 mm along the longitudinal direction of 30 mm to change its local resonant frequency with respect to the position. A detecting electrode array with 24-elements of 0.50 × 1.0 mm rectangles is made of an aluminum thin film on ABM, where they are located in a center line of longitudinal direction with the gaps of 0.50 mm. Since the device will be implanted into a cochlea filled with lymph fluid in future, the basic characteristics in terms of vibration and acoustic/electric conversion are investigated both in the air and in the silicone oil which is a model of lymph fluid. The in vitro optical measurements show that the local resonant frequency of vibration is varied along the longitudinal direction from 6.6 to 19.8 kHz in the air and from 1.4 to 4.9 kHz in the silicone oil, respectively. Since a resonating place vibrates with relatively large amplitude, the electric output there becomes high and that at the other electrodes remains to be low. Thus, the electric voltages from each electrode realize the frequency selectivity. Furthermore, the effect of surrounding fluid on the vibration is discussed in detail by comparing the experimental results with the theoretical predictions obtained by the Wentzel–Kramers–Brillouin asymptotic method. The theoretical prediction indicates that the surrounding fluid of the higher density induces the larger effective mass for the vibration that results in lower resonant frequency. From these findings, the feasibility of artificial cochlea is confirmed both experimentally and theoretically.

© 2009 Elsevier B.V. All rights reserved.

1. Introduction

The sensorineural hearing loss is a type of deafness which is often caused by the damage on hair cells of cochleae in inner ears. The hair cells convert acoustic sounds to electric signals that stimulate auditory nerves. As a clinical treatment for the hearing loss in children and adults, the artificial cochlea is recently well used. The device bypasses the damaged hair cells by generating the electric current in response to the acoustic sound [1,2]. The current artificial cochlea consists of an implantable electrode array for the stimulation and an extracorporeal device including a microphone, a sound processor and a battery. The acoustic sound is detected and is analyzed with respect to the frequency by the extracorporeal device. The processed signals are transferred through a transcutaneous system. Then, the auditory nerves are stimulated through the electrodes inserted in the cochlea. The disadvantages in the current system are the indispensability of extracorporeal devices, the small number of electrodes which closely connects to the limitation of tones, and the relatively large power consumption. This situation motivates us to develop a fully self-contained implantable artificial cochlea.

The important functions of cochlea are not only the conversion of acoustic wave to electric signals but also the frequency selectivity [3,4]. The basilar membrane which is a biological diaphragm in the cochlea plays an important role for the frequency selectivity. The local eigen frequency of membrane is changing along the place

* Corresponding author. Tel.: +81 6 6850 6179; fax: +81 6 6850 6179.
E-mail address: shintaku@me.es.osaka-u.ac.jp (H. Shintaku).

0924-4247/$ – see front matter © 2009 Elsevier B.V. All rights reserved.
doi:10.1016/j.sna.2009.12.021

Nomenclature

A_j	Fourier coefficient
$b(x)$	width of ABM, m
D	bending rigidity, N m
E	Young's modulus, Pa
f	frequency, Hz
h	thickness of ABM, m
$k(x)$	wave number, m^{-1}
L_1	width of fluid channel, m
L_2	depth of fluid channel, m
L_3	length of ABM, m
p_f	pressure, Pa
w	displacement of ABM, m
$W(x)$	envelope function, m
(x, y, z)	Cartesian coordinates, m

Greek letters

$\eta(x, y)$	shape function for ABM's bending in y direction
ν	Poisson ratio
ρ_f	density of fluid, kg m^{-3}
ρ_m	density of PVDF, kg m^{-3}
$\phi_f(x, y, z, t)$	velocity potential, m^2/s
ω	angular frequency, rad/s

Subscripts

f	region of fluid channel f = l or u
j	mode number of Fourier coefficient
l	lower fluid channel
m	PVDF
u	upper fluid channel

of it, because of varying mechanical boundary conditions and the mechanical rigidity. Thus, when the eigen frequency at a local place match to that of acoustic wave, the place vibrates with relatively large amplitude due to the resonance. The vibration stimulates hair cells especially at the resonated place. As a result, the frequency of acoustic wave is recognized as the difference in tones.

To artificially realize the frequency selectivity, some microscaled devices have been reported. Tanaka et al. [5] and Xu et al. [6] developed acoustic sensors with the function of frequency selectivity by the use of resonance of cantilever arrays. Those sensors were evaluated in the atmospheric environment. Chen et al. [7] developed a beam array fixed on a trapezoidal channel and investigated the vibrating characteristics in the water. Despite the frequency selectivity of cantilevers or beams, their mechanical strength may not be enough for the implantation as the artificial cochleae for the long period. On the other hand, White and Grosh [8] developed a device made of polyimide membrane with Si_3N_4 beams. The demonstration for the frequency selectivity was conducted at the higher frequency range compared with the audible one. Wittbrodt et al. [9] also developed a device made of polyimide membrane with Al beams. They reported that the device possessed some similarities with the biological cochlea in terms of traveling waves, the frequency to place tonotopic organization, and the roll off beyond the characteristic place.

The acoustic sensor which is developed in this paper realizes both the frequency selectivity and the conversion of acoustic wave to the electric signal in the liquid environment without an external energy supply. The device is designed as a prototype model to test the basic concept of the acoustic sensor for the development of the self-contained implantable artificial cochlea. The device consists of a piezoelectric membrane fixed on a trapezoidal slit, where the membrane over the slit works as a detector. We name this trapezoidal membrane as an artificial basilar membrane (ABM). Discrete electrodes are fabricated on ABM by technologies of micro electromechanical systems (MEMS) to measure the electric signals generated in response to the externally applied acoustic waves. To model the liquid environment, the fluid channel which locates under ABM is filled with a silicone oil as a model of lymph fluid in the cochlea. The ABM's vibration is measured using a laser Doppler vibrometer (LDV) at the various frequencies in the range of 1.0–20 kHz. The electric output is measured through the electrodes using a preamplifier. To predict the performance of the present device, the oscillatory dynamics of ABM is theoretically analyzed based on the vibrating equation of a thin plate bending and equations for the fluid dynamics. The phenomenon of fluid-structure interaction is treated by coupling those basic equations. To treat the wave motion on trapezoidal ABM, the Wentzel–Kramers–Brillouin (WKB) asymptotic solution [10] is used under the assumption of the gradually varying wavelength. The comparison between the experimental and theoretical results makes clear the detailed mechanism underlying the frequency selectivity. In addition, discussions for the further development as an implantable artificial cochlea are described from the viewpoint of magnitude of electric signal and the device size.

2. Principles and experimental methods

2.1. Basic mechanism of frequency selectivity and electric signal generation

A schematic and a photograph of piezoelectric acoustic sensor developed here are shown in Fig. 1. The device comprises a polyvinylidine difluoride (PVDF) membrane (KUREHA, Japan) bonded on a stainless plate with a trapezoidal slit and discrete electrodes distributed along x axis. PVDF is a piezoelectric material which can convert mechanical stresses to electric signals. The trapezoidal slit is designed so that the membrane over it, i.e. ABM, can be easily vibrated by the acoustic wave. The width $b(x)$ of ABM is linearly varied in the ranges of 2.0–4.0 mm along x of 30 mm long. This shape is intended to mimic the passive basilar membrane, that is, the local resonant frequency (LRF) of ABM gradually changes due to the varying mechanical boundary conditions along x. LRF is expected to be decreased as x increases. Applying acoustic wave with a certain frequency to ABM, a local place vibrates with relatively large amplitude due to the resonance. Electric signals are generated by the piezoelectric effect with respect to the local stress in ABM. Thus, the electrode on the resonating place gives a relatively large electric output. This is the basic mechanism of frequency selectivity realized by the association of resonance of vibration and the discrete electrode array. The device is mounted on a substrate with a fluid channel, where the channel dimensions are 47 × 17 mm rectangle and 4 mm deep. To model an in vivo environment, the fluid channel is filled with silicone oil (Shin-Etsu Chemical, Japan). The density and the viscosity of silicone oil are 873 kg/m^3 and 1.75×10^{-3} Pa s, respectively, where those of lymph fluid in cochleae are typically reported as 1.0×10^3 kg/m^3 [11] and from 1.0×10^{-3} to 1.97×10^{-3} Pa s [12,13], respectively. Although the both sides of basilar membrane in vivo face to the lymph fluid, in this experiment, only the bottom side of ABM faces to the silicone oil for the stable optical measurement from the upper side. The effect of this simplification is discussed by the theoretical analysis in the later section. Furthermore, the size of this ABM is relatively large to be implanted into the human cochlea. However, the main purpose of this paper is to test the basic mechanism of proposed system in terms of acoustic/electric conversion and the frequency selectivity. The optimization and the miniaturization will be remained as a future work. The advantages of miniaturized ABM are again discussed in later section.

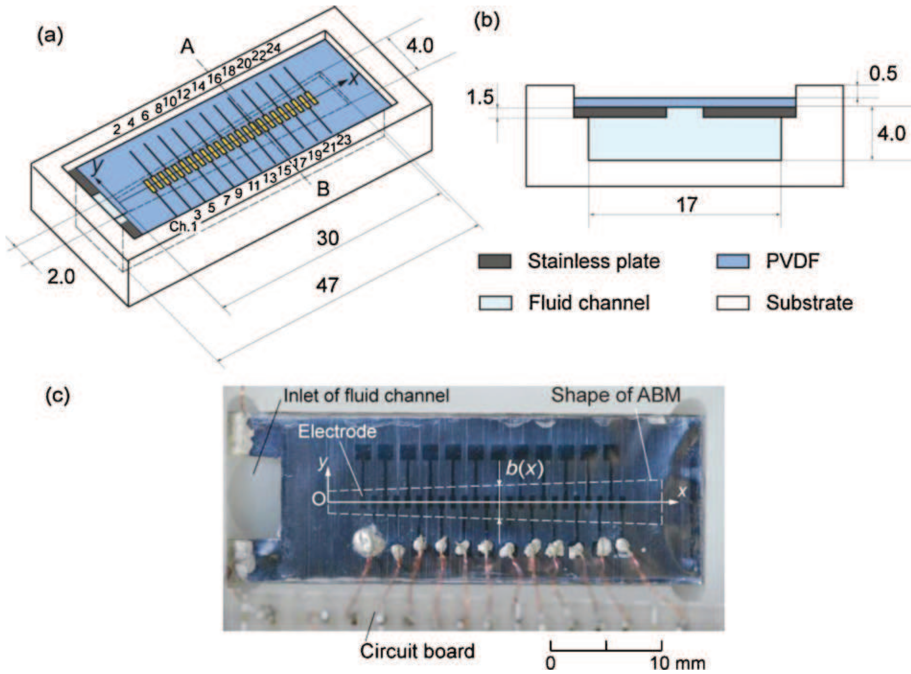

Fig. 1. Schematic and photograph of piezoelectric acoustic sensor; (a) 3D view, (b) cross sectional view at AB, and (c) photograph (Unit: mm).

2.2. Experimental setup

The electrode array with 24 elements made of an aluminum thin film is fabricated on an upper side of a 40 μm thick PVDF membrane based on a standard photolithography and an etching process. For convenience, the electrodes are named as Ch.1–Ch.24 as shown in Fig. 1(a). The each electrode of 0.50 × 1.0 mm rectangular shape is equally spaced 1.0 mm center to center, resulting in a gap of 0.50 mm between two adjacent electrodes. The ground electrode is prepared as a common one for all discrete electrodes on the lower side of ABM. The membrane is glued on the stainless plate to be the trapezoidal ABM. Since the electrodes of about 100 nm thick are extremely thinner than the PVDF of 40 μm, they may not strongly affect on the vibrating characteristics of ABM.

Fig. 2 shows a schematic of experimental setup. The sinusoidal acoustic wave is applied to the device from a speaker (FOSTEX, Japan) which is located 120 mm distant with 45° at a tilt. The speaker is previously calibrated to realize the constant sound pressure with the precision of ±0.1 dBSPL at various frequencies. The frequency is controlled by the function generator (NF, Japan) from 1.0 to 20 kHz which is in the range of audible frequency. The device on the substrate is set on a motorized stage which moves x and y directions for the measurement of spatial distribution of vibration amplitude. The velocity of ABM in z due to the vibration by the acoustic wave is measured by the LDV (Graphtec, Japan). The displacement, which is converted from the velocity data, is analyzed by an FFT to obtain the amplitude of vibration at the frequency of acoustic wave. At the same time, the piezoelectric output from the electrodes is measured in terms of voltage using a preamplifier and an oscilloscope.

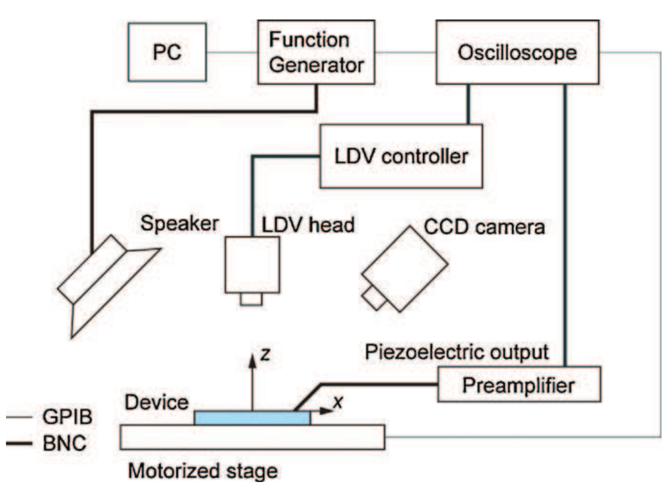

Fig. 2. Schematic of experimental setup for measurement of vibrating characteristics of ABM.

2.3. Oscillatory dynamics of artificial basilar membrane

Because the phenomena including the fluid-structure interaction are relatively complex, it is important for practical engineering to develop a theoretical model that effectively and easily predicts the vibrating characteristics of ABM. To obtain a mathematical solution, the following assumptions are made based on the experimental observations.

(1) The vibration of ABM is modeled as the bending vibration of a thin plate with small-amplitudes. The plain stress condition is valid, since the thickness h of ABM is small compared with the width or length.
(2) The fluid flow is assumed as incompressible, since $O(\omega^2 L^2/c^2)$ is 10^{-2}–10^{-6}, where the angular frequency ω is $O(10^3)$–$O(10^5)$, the characteristic length L is $O(10^{-3})$, and the sound velocity c is $O(10^3)$.
(3) The effects of gravity and viscosity of surrounding fluid are ignored.

The governing equation for the bending vibration of a plate with isotropic mechanical properties can be described as

$$\rho_{\mathrm{m}} h \frac{\partial^2 w}{\partial t^2} + D\left[\frac{\partial^4 w}{\partial x^4} + 2\frac{\partial^4 w}{\partial x^2 \partial y^2} + \frac{\partial^4 w}{\partial y^4}\right] = p_0 \quad (1)$$

where D, p_0, w, and ρ_m are the bending rigidity, the pressure of acoustic wave, the displacement in z direction, and the density of ABM, respectively. The bending rigidity D is related to Young's modulus E as

$$D = \frac{Eh^3}{12(1-\nu^2)} \tag{2}$$

where ν is the Poisson ratio.

The basic equation for the fluid flow is the Laplace equation of velocity potential ϕ_f as

$$\frac{\partial^2\phi_f}{\partial x^2} + \frac{\partial^2\phi_f}{\partial y^2} + \frac{\partial^2\phi_f}{\partial z^2} = 0 \tag{3}$$

The velocity potential ϕ_f is related to the velocity components (u_x, u_y, u_z) as

$$u_x = \frac{\partial\phi_f}{\partial x}, \quad u_y = \frac{\partial\phi_f}{\partial y}, \quad u_z = \frac{\partial\phi_f}{\partial z} \tag{4}$$

respectively. The subscript f is u or l, where u and l indicate the fluid at the upper and lower sides of ABM, respectively. Furthermore, the velocity potential ϕ_f is related to the pressure as

$$\rho_f \frac{\partial\phi_f}{\partial t} = -p_f \tag{5}$$

where ρ_f is the density of fluid.

The governing equations are solved with the following boundary conditions. The normal velocities at the wall of fluid channel are written as

$$u_z = \frac{\partial\phi_l}{\partial z} = 0 \quad \text{at} \quad z = -L_2 \tag{6}$$

$$u_y = \frac{\partial\phi_l}{\partial y} = 0 \quad \text{at} \quad y = \pm\frac{L_1}{2} \tag{7}$$

where L_1 and L_2 are the width and the depth of fluid channel, respectively. The kinematic boundary condition at $z = 0$ is written as

$$\frac{\partial w}{\partial t} = \frac{\partial\phi_f}{\partial z} \quad \text{at} \quad z = 0 \tag{8}$$

The thickness h of ABM is ignored in the analysis of fluid flow, since it is relatively small compared with the depth L_2 of fluid channel. The pressure p_0 is the pressure difference between the upper and lower sides of ABM and can be written as

$$p_0 = -\rho_l \frac{\partial\phi_l}{\partial t} + \rho_u \frac{\partial\phi_u}{\partial t} \quad \text{at} \quad z = 0 \tag{9}$$

Since ρ_l is extremely large compared with ρ_u in the present experiment, Eq. (9) is approximated as

$$p_0 \cong -\rho_l \frac{\partial\phi_l}{\partial t} \quad \text{at} \quad z = 0 \tag{10}$$

To obtain the oscillatory solution at the periodic steady state, following assumptions are made.

(4) A single mode $\eta(x, y)$ is used for the shape function of ABM's bending in y direction. $\eta(x, y)$ is determined based on the analytical solution of a vibrating beam with the first mode, the length of $b(x)$, and the fixed boundary conditions at $y = \pm b(x)/2$ as

$$\eta(x,y) = \begin{cases} c_1 \cos\left(\dfrac{\beta}{b(x)}y\right) + c_2 \cos h\left(\dfrac{\beta}{b(x)}y\right) & \text{at } -\dfrac{b(x)}{2} \le y \le \dfrac{b(x)}{2} \\ 0 \quad \text{at } -\dfrac{L_1}{2} \le y \le -\dfrac{b(x)}{2} \quad \text{and} \quad \dfrac{b(x)}{2} \le y \le \dfrac{L_1}{2} \end{cases} \tag{11}$$

where c_1, c_2, and β are constants of 0.8827, 0.1173 and 4.730, respectively. These constants are determined to make $\eta(x, y)$ satisfy the fixed boundary conditions at $y = \pm b(x)/2$.

(5) The wave is considered as a slowly varying wave in x direction. That is, the wave number $k(x)$ is slowly varying along x as $b(x)$, where $db(x)/dx \cong 0$ and $dk(x)/dx \cong 0$ are reasonable in the scale of a one wavelength. In this case, the waves can be treated as pseudo plane ones and can be described by the WKB asymptotic solution [10].

Based on these assumptions described above, the displacement $w(x, y, t)$ of ABM can be written as

$$w = W(x)\,\eta(x,y)\,e^{i\int_0^x k(\xi)d\xi} e^{-i\omega t} \tag{12}$$

where i and $W(x)$ are the imaginary number and the envelope function, respectively. $W(x)$ is also treated as a slowly varying function, that is $dW(x)/dx \cong 0$, since the effect of $dW(x)/dx$ on the dispersion relationship is trivial for linear problems [14]. The main purpose of the theoretical analysis is to predict the distribution of the local resonant frequency and to clarify the effect of the surrounding fluid on the resonance. Therefore, to simplify the mathematical development, only the forward wave is included in the analysis. On the other hand, the solution for Eq. (3) which satisfies the boundary conditions of Eqs. (6) and (7) is written as

$$\phi_l = \sum_{j=0}^{\infty} A_j \cos h\left[\zeta_j(z + L_2)\right] \cos\left(\frac{j\pi}{L_1}y\right) e^{i\int_0^x k(\xi)d\xi} e^{-i\omega t} \tag{13}$$

where A_j and ζ_j are the Fourier coefficient for jth mode and $[k^2(x) + (j\pi/L_1)^2]^{1/2}$, respectively. From Eqs. (8), (12) and (13), the following equation is obtained:

$$i\omega W(x)\eta(x,y) = -\sum_{j=0}^{\infty} A_j\zeta_j \sin h(\zeta_j L_2)\cos\left(\frac{j\pi}{L_1}y\right) \tag{14}$$

Using the orthogonality of cosine function, A_j is calculated as

$$A_j = -\frac{i\omega W(x)\int_{-b(x)/2}^{b(x)/2} \eta(x,y)\cos\left(j\pi y/L_1\right)dy}{\zeta_j \sin h\left(\zeta_j L_2\right)\int_{-L_1/2}^{L_1/2} \cos^2\left(j\pi y/L_1\right)dy} \tag{15}$$

Eqs. (10) and (12) are substituted into Eq. (1). Then, multiplying $\eta(x, y)$ to Eq. (1), and integrating from $-b(x)/2$ to $b(x)/2$ with respect to y, the following eikonal equation is obtained:

$$\begin{aligned} f(x,\omega) &= D\left[k^4(x)\int_{-b(x)/2}^{b(x)/2}\eta^2(x,y)\,dy - 2k^2(x) \right.\\ &\quad \left.\times \int_{-b(x)/2}^{b(x)/2}\eta(x,y)\,\partial^2\eta(x,y)/\partial y^2 dy + \left[\beta/b(x)\right]^4\int_{-b(x)/2}^{b(x)/2}\eta^2(x,y)\,dy\right] \\ &\quad -\omega^2\left[\rho_m h\int_{-b(x)/2}^{b(x)/2}\eta^2(x,y)\,dy + \rho_l\sum_{j=0}^{\infty}\frac{\left[\int_{-b(x)/2}^{b(x)/2}\eta(x,y)\cos\left(j\pi y/L_1\right)dy\right]^2}{\zeta_j \tan h\left(\zeta_j L_2\right)\int_{-L_1/2}^{L_1/2}\cos^2\left(j\pi y/L_1\right)dy}\right] \end{aligned} \tag{16}$$

Eq. (16) describes the dispersion relationship between $k(x)$ and ω at various x. The effect of surrounding fluid is found in the last term of Eq. (16). Since this term contributes to increase the effective mass for the vibration, the resonant frequency may be decreased by the surrounding fluid. From the average variation principle [14], it is known that the eikonal equation has the relationship with $W(x)$ as

$$W(x) = \frac{c}{\left(\frac{\partial f}{\partial k}\right)^{1/2}} \tag{17}$$

Table 1
Parameters for prediction.

Parameter	Symbol	Value
Width of ABM (m)	$b(x)$	$b(x) = 0.002 + 0.002x/L_3$
Young's modulus of PVDF (Pa)	E	3×10^{9} [a]
Width of fluid channel (m)	L_1	0.017
Depth of fluid channel (m)	L_2	0.004
Length of ABM (m)	L_3	0.03
Poisson ratio of PVDF	ν	0.29 [a]
Density of PVDF (kg/m^3)	ρ_m	1780 [15]
Density of silicone oil (kg/m^3)	ρ_s	873 [b]
Density of air (kg/m^3)	ρ_a	1.2 [16]

[a] From technical report by KUREHA.
[b] From technical report by Shin-Etsu Chemical.

where c is a constant. Eq. (17) is the transport equation which describes the qualitative distribution of $W(x)$.

The parameters for the prediction are listed in Table 1. If the angular frequency ω is given as that of externally applied acoustic wave, only the wave number $k(x)$ is a variable to be solved in Eq. (16), where Eq. (16) is reduced to $f(k(x)) = 0$. At various ω, Eq. (16) is solved numerically by the Newton method. The iteration procedure is repeated until the residual becomes less than a specified tolerance of 10^{-6}. The term including summation is treated from $j = 0$ to 30, which is adequate for the tolerance. The calculation is conducted for the two cases of filling the fluid channel with the air and of that with the liquid. The frequency is changed in the ranges of 3.5–14.0 kHz in the air environment and 0.7–3.6 kHz in the liquid environment, respectively. At those frequencies, Eq. (16) gives solutions and $W(x)$ has a peak on ABM.

Fig. 3 shows $W(x)$ which describes the qualitative amplitude distribution defined by Eq. (17). $W(x)$ in the air environment of Fig. 3(a) shows a clear peak at each frequency, where the peak indicates the resonance at the local place. Comparing $W(x)$ at different frequencies, it is found that the peak position shifts to smaller x as the frequency increases. It is also found that the peak value of $W(x)$ decreases as the frequency increases. Fig. 3(b) shows the $W(x)$ in the liquid environment. As same with the result in the air environment, the peak position shifts to smaller x as the frequency increases. However, compared with the results in the air environment, $W(x)$ in the liquid environment shows peaks at smaller frequencies. By comparing the results at 3.5 kHz in Fig. 3(a) and (b), the effect of the surrounding fluid on $W(x)$ can be discussed in detail. Although ABM is vibrated at the same frequency, it is found that the peak position in the liquid environment is shifted to smaller x and the form of $W(x)$ is moderated compared with those in the air environment. These results indicate that the stronger fluid-structure interaction due to the higher density decreases the resonant frequency and relaxes the resonance. Based on Eq. (16), the mechanism of decreasing the resonant frequency in the liquid environment is that the effective mass for the vibration is increased due to the much higher density of the liquid compared with that of the air. The reason for the moderated resonance is discussed later.

Fig. 4(a) shows the distributions of $k(x)$ in the air environment at 3.5, 6.0, 9.0, and 12.0 kHz. In Fig. 4(a), it is found that $k(x)$ in the air environment increases with x. There is a certain position of x_{inc} where $k(x)$ rapidly increases. x_{inc} is mathematically defined as the position where $k(x)$ gives the largest gradient. At larger x than x_{inc}, $O(k(x))$ is 10^2–10^3 m^{-1} and the wavelength is 63–6.3 mm. At smaller x than x_{inc}, $k(x)$ is very small which corresponds to the extremely long wavelength. Comparing the results at different frequencies, it is found that x_{inc} becomes smaller at the higher frequency. It is also found that x_{inc} is close to the peak position of $W(x)$ in Fig. 3(a). Since the result is obtained by the analysis based on the WKB solution, the wavelength should be short enough to treat $b(x)$ as a slowly varying function. Furthermore, $k(x)$ should be gradually changed by x. Thus, the precision of result should be relatively bad around x_{inc} and at smaller x than x_{inc}. Fig. 4(b) shows the $k(x)$ distributions in the liquid environment at 1.0, 2.0, 3.0, and 3.5 kHz. $k(x)$ in the liquid environment gradually increases with x compared with that in the air environment. Although the resonant frequencies are different between in the air and in the liquid envi-

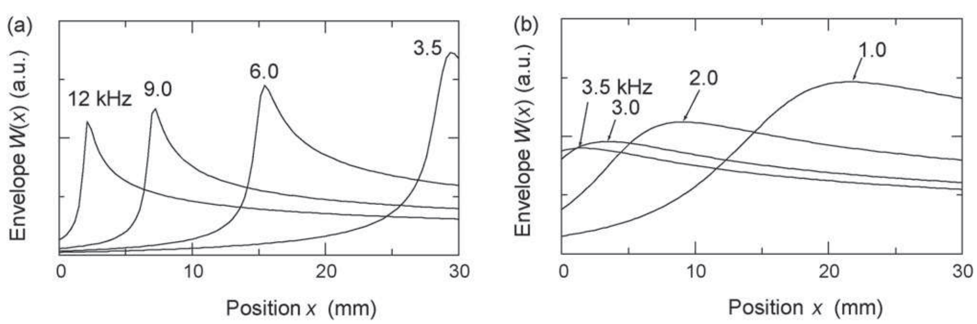

Fig. 3. Theoretical results of envelope function $W(x)$ in (a) air and in (b) liquid environments for various frequencies.

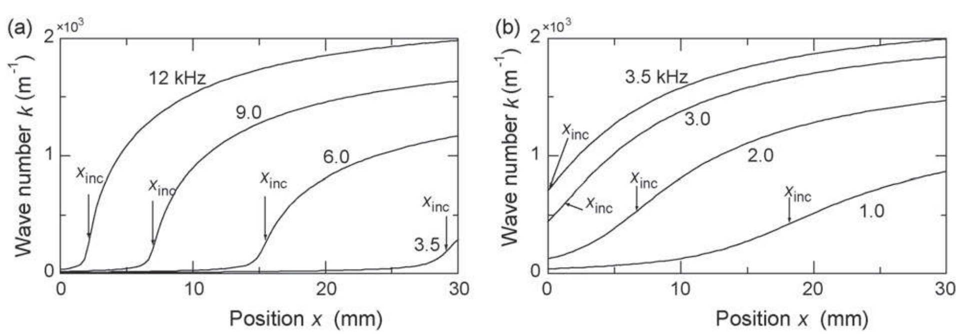

Fig. 4. Theoretical results of wave number $k(x)$ in (a) air and in (b) liquid environments for various frequencies.

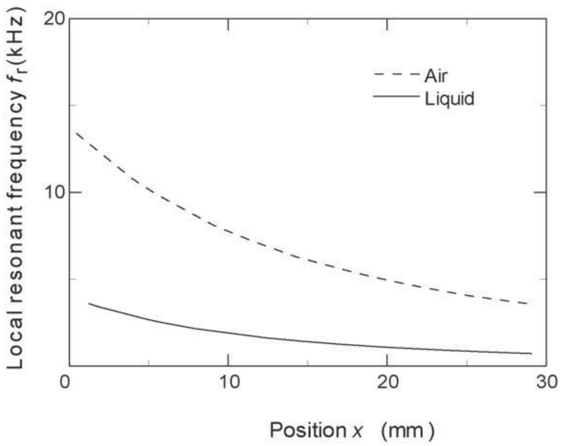

Fig. 5. Theoretical results of local resonant frequencies in air and in liquid environments.

ronments, the orders of $k(x)$ around x_{inc} and at larger x than x_{inc} are similar to the results in the air environment. From this result, it can be said that the resonance is governed by the wavelength which is strongly related to the geometry of ABM. x_{inc} is closely connected with the peak position of $W(x)$ shown in Fig. 3(b). Furthermore, the reason for the moderated resonance in the liquid environment can be explained by comparing Fig. 4(a) and (b). Since $k(x)$ in the air environment rapidly changes around the resonance place as shown in Fig. 4(a), the evolution of $W(x)$ also does. It is owing to the fact that the resonance condition is governed by the wavelength. On the contrary, since $k(x)$ in the liquid environment gradually changes around the resonance place as shown in Fig. 4(b), the peak of $W(x)$ becomes to be moderated.

Fig. 5 shows the relationship between the resonant frequency f_r and x. Both f_r in the air and in the liquid environments decrease as x increases and f_r in the liquid environment is lower than that in the air environment due to the increase of effective mass. Although the auditory frequency is widely ranged from 20×10^{-3} to 20 kHz, the device can cover only the part of it. It works at the frequencies over the ranges of 3.5–14 kHz in the air environment and 0.7–3.6 kHz in the liquid environment, respectively. For the clinical application, the device should be optimized to realize the frequency selectivity in the required frequency range for a daily conversation. Furthermore, distribution of f_r should be fitted to that in the biological system from the viewpoint of natural hearing. To solve these problems, the geometrical optimizations of ABM can be effectively carried out in our future work based on the theoretical analysis developed here.

The theoretical analysis is carried out based on the experimental condition, where only the bottom side of ABM faces to the liquid. In case of ABM facing to the liquid at both sides, the difference is found in the last term of Eq. (16) which includes the effect of surrounding fluid. In case of the same fluid channel is placed on the upper side of ABM and is filled with the same liquid, the last term is double of that in Eq. (16). Consequently, the larger effect of surrounding fluid is induced, that is, the further decrease of resonant frequency is found due to the increase of effective mass for the vibration, where the figure is omitted.

Furthermore, the theoretical analysis is carried out based on the assumption of the small amplitude. The basic equations are solved by WKB treatment which cannot quantitatively predict the vibrating amplitude. Therefore, it is difficult to precisely estimate the piezoelectric output which is determined by the strain in the membrane. The investigation on the piezoelectric output can be made by the numerical analysis based on the finite element method, which is our future research.

3. Results and discussion

3.1. Performance test in air environment

The basic vibrating characteristics of ABM in the air environment are investigated as a preliminary experiment. This experiment is conducted without filling the fluid channel with the silicone oil. The amplitude distributions of vibration are measured by applying acoustic waves of 75 dBSPL. The frequency is controlled over the range of 1.0–20.0 kHz, which covers the part of human's audible frequency. The amplitude of vibration becomes relatively small at the frequencies both lower than 3.0 kHz and higher than 18.0 kHz. It may be owing to that ABM is designed to have LRF for the first mode over the range of 3.5–14.0 kHz in the air environment. Fig. 6(a)–(d) show the amplitude distribution at f = 4.0, 6.0, 9.0, and 12.0 kHz, respectively. The amplitude distribution clearly shows dependence on the frequency. The place with maximum amplitude, where ABM is locally resonating, shifts to the smaller x as the frequency increases. This relationship between the position of resonating place and the frequency successfully has similarities with that of biological basilar membranes. Furthermore, in Fig. 6(c) and (d), it is found that there are several extrema indicated by arrows at the larger x than that of resonating place. These may be induced by the standing wave due to the traveling waves to positive and negative directions of x. The reason why the standing wave is not observed at the smaller x than that of resonating place is that the wavelength is relatively long at those positions. This is confirmed by the theoretical result of relatively small $k(x)$ as shown in Fig. 4(a). In the biological cochlea, the acoustic wave travels from the basal to the apex. However, in our experiment, it is applied to the entire ABM from the air. As a result, the relatively large effects of the standing waves are induced in our experiment due to the small damping effects from the surrounding fluid.

Fig. 7(a)–(c) show the frequency dependences of vibration and the piezoelectric output at Ch. 6, Ch. 12 and Ch. 18, respectively. The amplitudes of vibration and the piezoelectric output are plotted by a solid line and by a broken line, respectively. It seems that each electrode has a specific frequency where the electrode gives

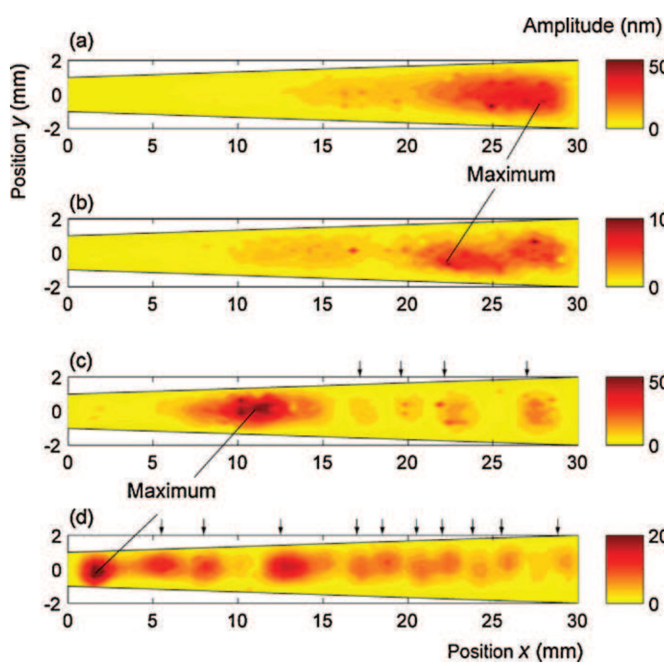

Fig. 6. Experimental results of contour maps of vibration amplitude at (a) f = 4.0 kHz, (b) 6.0 kHz, (c) 9.0 kHz, and (d) 12.0 kHz in air.

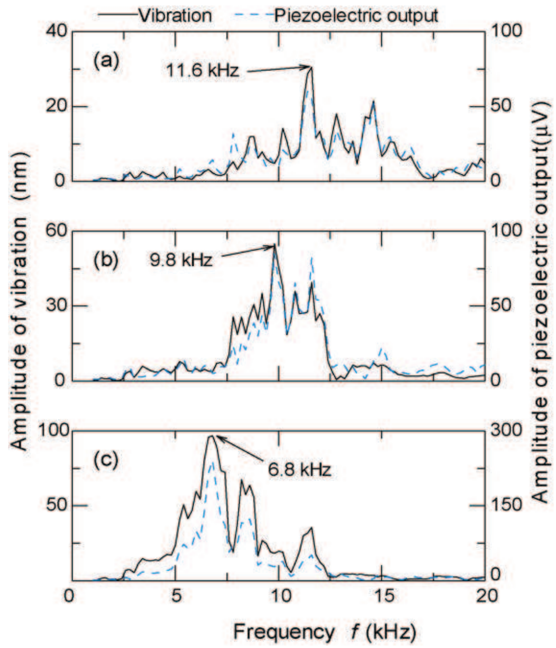

Fig. 7. Experimental results of vibration amplitude and piezoelectric output from (a) Ch. 6, (b) Ch. 12 and (c) Ch. 18 at various frequencies in air.

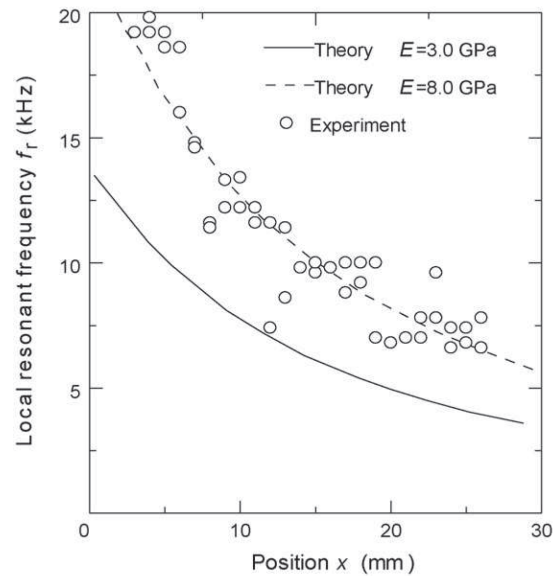

Fig. 8. Comparison of theoretically and experimentally obtained results of local resonant frequency f_r in air.

relatively large outputs. The specific frequency is defined as LRF of electrode. LRF decreases as the channel number increases, i.e., as the position x increases. Extremal amplitudes at other frequencies of LRF may indicate the effect of standing waves. That is, in case of the electrode locates on the antinode of standing wave, the amplitude from the electrode increases. On the other hand, in case of the electrode locates on the node, the amplitude decreases. As reported in Refs. [7,8,17], pretension in the membrane may be a main reason for the standing wave which results in the multiple-peaks as shown in Fig. 7. However, it is difficult to precisely control the pretension in our fabrication process. Therefore, the mechanism of this result remained to be solved in this study. The frequency dependences of vibration and the piezoelectric output are qualitatively similar to each other. The reason of their similarity can be explained as follows. Since ABM is relatively narrow in y direction compared with that in the x direction, the vibration is mainly effected by the boundary conditions at $y = \pm b(x)/2$. As the result of that, the piezoelectric output is dominated by the ABM's local structural strain in y direction. Furthermore, the piezoelectric constant in y direction is larger than that in x direction. This may make the strong dependence of piezoelectric output on the strain in y direction.

Fig. 8 shows the relationship between LRF f_r and position x. Circles are LRF which are determined by the vibration and the piezoelectric output. LRF decreases from 19.8 to 6.6 kHz as x increases. This experimental LRF is in qualitative agreement with the theoretical prediction of Eq. (16) which is drawn by the solid line. In the quantitative comparison, however, almost all experimental results are slightly higher than the predictions. One of possible reasons is the underestimation of E. Since E from literatures widely distributes as 3.0–11.0 GPa [18,19], we used a reference value of 3.0 GPa for the prediction. If we use higher value of 8.0 GPa, the precision is improved as shown by the broken line in Fig. 8.

Fig. 9(a) shows the relationship between the external sound pressure and the amplitude of vibration in ABM. This investigation is conducted at LRF of each electrode. To show the results over the range of 60–90 dBSPL, those are drawn in the log-dBSPL plot. From the gradient of results, it is found that the amplitude of vibration at LRF linearly increases with the sound pressure. The amplitude increases with the channel number, that is, with ABM's width. Fig. 9(b) shows the relationship between the sound pressure and the amplitude of piezoelectric output. The amplitude of piezoelectric output also shows the linear relationship with the sound pressure. These results suggest that the device can detect not only the frequency of acoustic wave but also the magnitude of it.

3.2. Performance test in liquid environment

The performance of device in the liquid environment is investigated by filling the fluid channel with the silicone oil with the

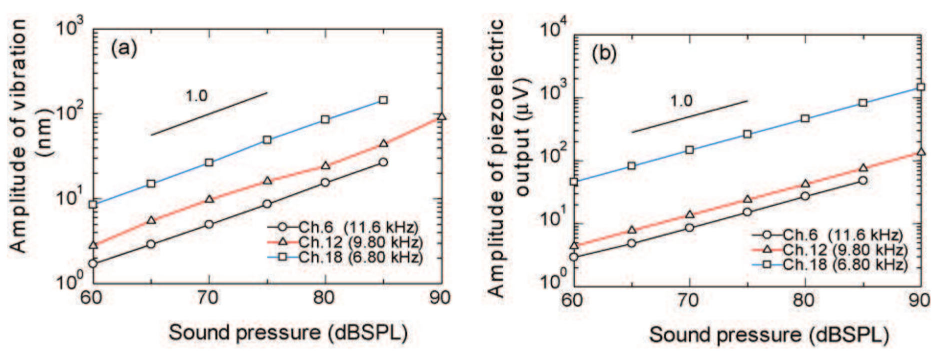

Fig. 9. Experimental results in effect of sound pressure on amplitudes (a) of vibration and (b) of piezoelectric output in air.

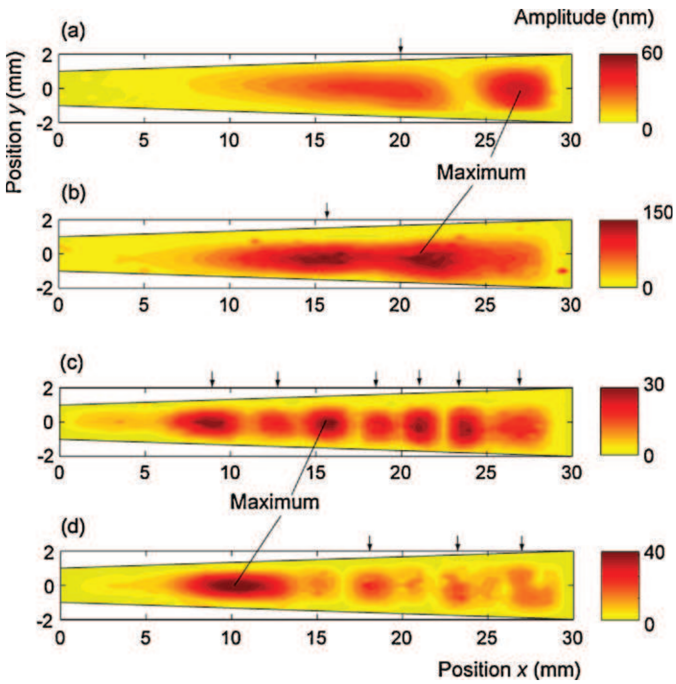

Fig. 10. Experimental results of contour maps of vibration amplitude at (a) f = 1.5 kHz, (b) 2.0 kHz, (c) 3.0 kHz and (d) 4.0 kHz in silicone oil of 1.75×10^{-3} Pa s.

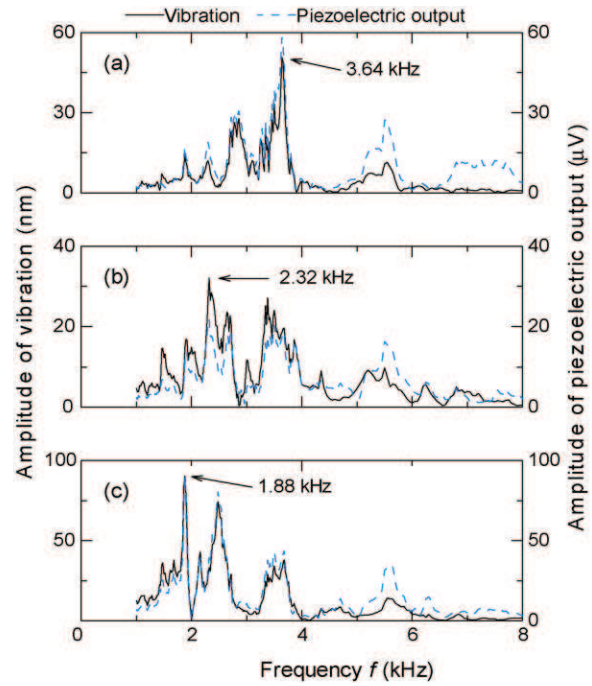

Fig. 11. Experimental results of vibration amplitude and piezoelectric output from (a) Ch. 6, (b) Ch. 12 and (c) Ch. 18 at various frequencies in silicone oil of 1.75×10^{-3} Pa s.

viscosity of 1.75×10^{-3} Pa s. This investigation is intended to test the applicability of device for implanting into the cochlea. Since the outputs from ABM are relatively small compared with that in the air environment, the sound pressure is increased to be 85 dBSPL for this experiment. This decrease of outputs in the silicone oil may be caused by energy dissipation in liquid environment due to the viscosity and the stronger fluid-structure interaction of ABM due to the density, however, the detailed mechanism has not been clarified. Fig. 10 shows the contour maps of amplitude distribution at (a)f = 1.5 kHz, (b)2.0 kHz, (c)3.0 kHz and (d) 4.0 kHz, respectively. The qualitative frequency dependence of vibration is similar to that in the air environment. That is, the location with the maximum amplitude is shifted to the smaller x as the frequency increases. However, the frequency ranges where ABM shows peak amplitude in the silicone oil are lower than that in the air environment. Comparing Fig. 6(a) and Fig. 10(d), the effect of surrounding fluid can be discussed in detail. In spite of driving the device at the same frequency of 4.0 kHz, these results clearly show the different vibration behavior. It is found that the maximum amplitude is found at the smaller x in the silicone oil compared with that in the air environment. This difference may be caused by the fluid-structure interaction as discussed in the earlier section. That is, compared with the result in the air environment, the effective mass for the vibration is increased in the silicone oil. As a result, the place with maximum amplitude is shifted to the smaller x in the silicone oil at the same frequency. Furthermore, the effects of standing wave in the silicone oil which are indicated by arrows seem relatively large compared with that in the air environment. This fact is predicted by the theoretical analysis that the resonance is relaxed due to the surrounding liquid as shown in Fig. 3.

Fig. 11 shows the frequency dependences of vibration and piezoelectric output, where they are indicated by a solid line and the broken one, respectively. As same with those in the air environment, the two amplitudes show the similar tendency to each other. The amplitudes have peaks at each specific frequency which is also described as LRF for convenience. LRF of Ch. 6, Ch. 12, and Ch. 18 are obtained as 3.64, 2.32, and 1.88 kHz, respectively. From Fig. 11, it is confirmed that the ABM's frequency selectivity is successfully realized even in the liquid environment. However, comparing Figs. 7 and 11, the peak height at the LRF becomes low, i.e., the selectivity seems worse than that in the air environment. This result qualitatively agrees with the theoretical result that the peak is relaxed in the liquid environment as shown in Fig. 3. In order to dramatically improve the frequency selectivity, it is expected that the sensor including the active feedback control which mimics the biological cochlea should be developed in future.

Fig. 12 shows the relationship between f_r and x in the silicone oil. From Fig. 12, it is found that the LRF decreases from 4.9 to 1.4 kHz as x increases, where the range is lower than that in the air environment. The experimentally obtained LRF is compared

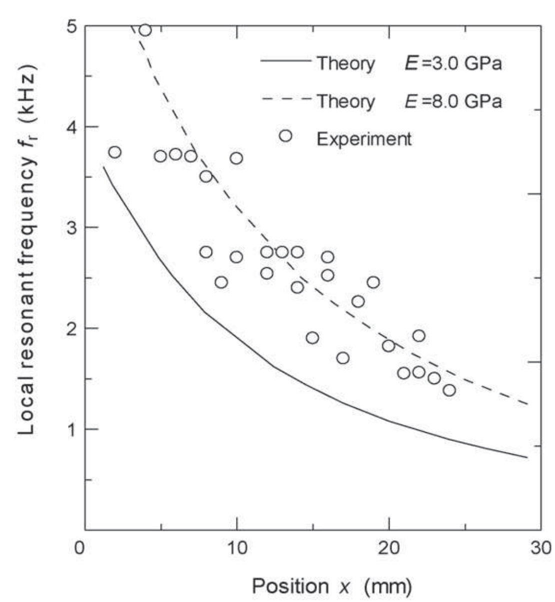

Fig. 12. Comparison of theoretically and experimentally obtained results of local resonant frequency f_r in silicon oil of 1.75×10^{-3} Pa s.

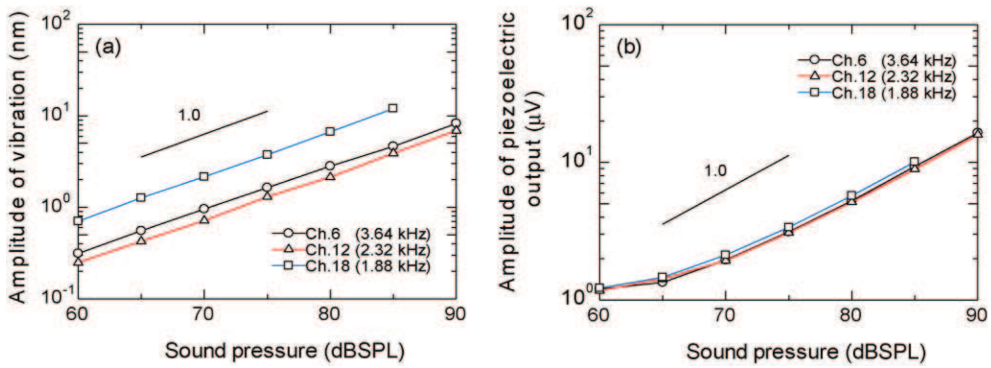

Fig. 13. Experimental results in effect of sound pressure on amplitudes (a) of vibration and (b) of piezoelectric output in silicone oil of 1.75×10^{-3} Pa s.

with the theoretically obtained one in Fig. 12. The predicted LRF of E = 8.0 GPa which is drawn by the broken line reasonably agrees with the experimentally obtained ones. From this agreement, it can be said that the theoretical analysis well reproduces the effect of the fluid-structure interaction on LRF. Since the theoretical analysis is carried out with inviscid fluid model, it can also be said that the decrease of LRF in the liquid environment is governed by the increase of effective mass for the vibration under the condition of constant sound pressure.

Fig. 13(a) shows the relationships between the sound pressure and the amplitudes of vibration. The amplitude of vibration linearly increases with the sound pressure. However, the amplitude of piezoelectric output shown in Fig. 13 (b) seems to be nonlinear especially at the low sound pressure level of 60–70 dBSPL. It may be due to the viscosity of liquid, however, it is difficult to confirm the reason for the nonlinear relationship due to the lack of the basic knowledge, where it is in our future work. As shown in Fig. 13(b), the amplitude of piezoelectric output is about 16 μV at 90 dBSPL in the silicone oil. The acoustic wave of 90 dBSPL is relatively loud for the normal hearing. Even applying such a high sound pressure, the developed device can generate several tens of μV at most. To effectively stimulate nerve cells [20], the electric output should be amplified. One of the methods for the amplification is to use equipment such as a hearing aid, where it amplifies the sound pressure. Another solution is the downsizing of device using a fully micromachining process, since the thinner membrane can generate the larger voltage. That is, the piezoelectric voltage V_p is proportional to the stress σ and the square of thickness h as $V_p \propto \sigma h^2$. On the other hand, the stress σ of ABM is inversely proportional to the cube of thickness as $\sigma \propto h^{-3}$. Consequently, the voltage is inversely proportional to the thickness as $V_p \propto h^{-1}$. The reduction of thickness can be easily realized by means of microfabrication and the thin films technologies. Thus, the implantable device will be developed based on those technologies in our future work.

3.3. Effect of viscosity on frequency selectivity

Fig. 14 shows the contour maps of amplitude distribution using the higher viscous silicone oil of 1.75×10^{-2} Pa s at (a)f = 1.5 kHz, (b)2.0 kHz, (c)3.0 kHz and (d) 4.0 kHz, respectively. The viscosity of the silicone oil is ten times higher than that in the previous section. The positions of maximum amplitude are x = 28.0, 24.0, 20.5, and 10.5 mm for f = 1.5, 2.0, 3.0, and 4.0 kHz, respectively as shown in Fig. 14. On the other hand, those are x = 27.0, 21.0, 16.0, and 10.0 mm in the results of 1.75×10^{-3} Pa s as shown in Fig. 10. From this result, it can be said that the effect of viscosity on the position of the resonating place seems small. It is also found that the local maximum amplitudes due to the standing wave are relatively small in Fig. 14 compared with those in Fig. 10. That is

Table 2
Ratio a_1/a_2 of height between the highest peak and the secondary highest one.

Frequency f (Hz)	Ratio at 1.75×10^{-3} Pa s a_1/a_2	Ratio at 1.75×10^{-2} Pa s a_1/a_2
1.5	1.52	1.69
2.0	1.03	1.56
3.0	1.08	1.96
4.0	1.89	2.08

quantitatively confirmed by the ratio a_1/a_2 which is the ratio of amplitudes between the highest peak a_1 and the secondary highest peak a_2 in Table 2. Comparing the results between 1.75×10^{-3} Pa s and 1.75×10^{-2} Pa s, it is found that the highest peak is significant in the higher viscous silicone oil. This may be caused because the wave is damped more rapidly in the higher viscous one. From the viewpoint of application, this result indicates that the effect of viscosity may contribute to improve the frequency selectivity. It is also possible to discuss the effect of viscosity by comparing the result between in the air and in the liquid environments. However, there are two different types of fluid-structure interactions of the increase in the effective mass and the viscous damping between

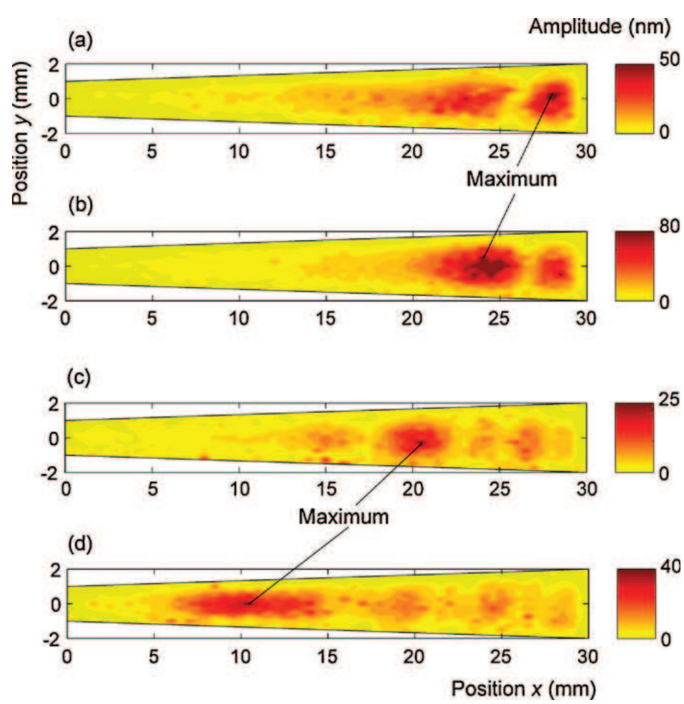

Fig. 14. Experimental results of contour maps of vibration amplitude at (a) f = 1.5 kHz, (b) 2.0 kHz, (c) 3.0 kHz and (d) 4.0 kHz in silicone oil of 1.75×10^{-2} Pa s.

those conditions. Since they contribute to the frequency selectivity oppositely, it is difficult to discuss separately. The development of theoretical analysis using full Navier-Stokes equation should be made in future research.

4. Concluding remarks

In this paper, we reported a novel piezoelectric artificial cochlea which worked as a sensor with the acoustic/electric conversion and with the frequency selectivity based on MEMS technology. The basic performances of prototype device both in the air and in the liquid environments were investigated experimentally and theoretically.

The vibrating characteristics of trapezoidal ABM were measured by applying acoustic waves at a certain frequency. The location with the maximum amplitude was shifted toward narrower area of trapezoidal ABM as the frequency increased. This phenomenon indicated that the developed device successfully realized the frequency selectivity.

The frequency dependences of vibration and piezoelectric output were investigated both in the air and in the silicone oil of 1.75×10^{-3} Pa s. The resonant frequencies were determined to be over the ranges of 6.6–19.8 kHz in the air and 1.4–4.9 kHz in the silicone oil, respectively. The decrease in the resonant frequency due to the silicone oil must be the effect of fluid-structure interaction, that is, the interaction between the acoustic wave in the fluid and the membrane vibration. The interaction contributed to increase the effective mass for the vibration. This consideration was confirmed by the reasonable agreement between the experiment and the theory in terms of local resonant frequency.

The viscous effect of surrounding fluid on the vibration was explored using the higher viscous silicone oil of 1.75×10^{-2} Pa s. The effect on the resonating place seemed to be small between 1.75×10^{-3} and 1.75×10^{-2} Pa s. However, it was found that the higher viscous liquid suppressed the standing wave and improved the frequency selectivity.

To develop the fully implantable device in our future work, the amplification of voltage may be required to effectively stimulate nerve cells. Furthermore, the present device is relatively large for the implantation into a cochlea. These problems can be solved by the use of microfabrication and thin films technologies. The miniaturization is accomplished by the technology straightforward. And the larger electric signals can be generated using the thinner ABM, since the voltage is expected to be inversed proportional to the thickness. As a matter of course, these further developments must be conducted considering the frequency dependence. Thus, the theoretical approach which is described here is useful to design it in our future work.

References

[1] F.G. Zeng, Trends in cochlear implants, Trends Amplification 8 (1) (2004) T1–T34.
[2] S.B. Waltzman, Cochlear implants: current status, Expert Rev. Med. Dev. 3 (5) (2006) 647–655.
[3] G.V. Békésy, Current status of theories of hearing, Science 123 (3201) (1956) 779–783.
[4] G.V. Békésy, Hearing theories and complex sounds, J. Acoust. Soc. Am. 35 (4) (1963) 588–601.
[5] K. Tanaka, M. Abe, S. Ando, A novel mechanical cochlea "fishbone" with dual sensor/actuator characteristics, IEEE ASME Trans. Mechatron. 3 (2) (1998) 98–105.
[6] T. Xu, M. Bachman, F.G. Zeng, G.P. Li, Polymeric micro-cantilever array for auditory front-end processing, Sens. Actuators A Phys. 114 (2–3) (2004) 176–182.
[7] F. Chen, H.I. Cohen, T.G. Bifano, J. Castle, J. Fortin, C. Kapusta, D.C. Mountain, A. Zosuls, A.E. Hubbard, A hydromechanical biomimetic cochlea: experiments and models, J. Acoust. Soc. Am. 119 (1) (2006) 394–405.
[8] R.D. White, K. Grosh, Microengineered hydromechanical cochlear model, Proc. Natl. Acad. Sci. U.S.A. 102 (5) (2005) 1296–1301.
[9] M.J. Wittbrodt, C.R. Steele, S. Puria, Developing a physical model of the human cochlea using microfabrication methods, Audiol. Neurootol. 11 (2) (2006) 104–112.
[10] C.R. Steele, L.A. Taber, Comparison of WKB calculations and experimental results for three-dimensional cochlear models, J. Acoust. Soc. Am. 65 (4) (1979) 1007–1018.
[11] J.D. Bronzino, The Biomedical Engineering Handbook, CRC Press, 1995.
[12] G. Zhou, L. Bintz, D.Z. Anderson, A life-sized physical model of the human cochlea with optical holographic readout, J. Acoust. Soc. Am. 93 (3) (1993) 1516–1523.
[13] J.H. ten Kate, J.W. Kuiper, The viscosity of the pike's endolymph, J. Exp. Biol. 53 (2) (1970) 495–500.
[14] G.B. Whitham, Linear and Nonlinear Waves, Wiley-Interscience, 1974.
[15] M. Chanda, S.K. Roy, Plastic Technology Handbook, CRC press, 2006, pp. 5–52.
[16] National Astronomical Observatory of Japan, Chronological scientific tables (2009), Maruzen.
[17] K.M. Lim, A.M. Fitzgerald, C.R. Steele, Building a physical cochlear model on a silicon chip, in: H. Wada, T. Takasaka, K. Ikeda, K. Ohyama, T. Koike (Eds.), Recent Developments in Auditory Mechanics, World scientific, 1999, pp. 223–229.
[18] J. Sirohi, I. Chopra, Fundamental understanding of piezoelectric strain sensors, J. Intell. Mater. Syst. Struct. 11 (4) (2000) 246–257.
[19] H. Ohigashi, Electromechanical properties of polarized polyvinylidene fluoride films as studied by the piezoelectric resonance method, J. Appl. Phys. 47 (3) (1976) 949–955.
[20] Y. Jimbo, T. Tateno, H.P.C. Robinson, Simultaneous induction of pathway-specific potentiation and depression in networks of cortical neurons, Biophys. J. 76 (2) (1999) 670–678.

Biographies

Hirofumi Shintaku received B.S., M.S., and Ph.D. degrees from Department of Mechanical Engineering, Kyoto University, Japan, in 2002, 2004, and 2006, respectively. Since 2006, he has been an Assistant Professor in Department of Mechanical Science and Bioengineering, Graduate School of Engineering Science, Osaka University, Japan. His current research area is fluid dynamics in the micro and nano meter scales.

Takayuki Nakagawa received M.D. and Ph.D. from Medical School, Osaka City University, Japan in 1989 and 1995, respectively. From 1995 to 2001, he was a Department Director in Department of Otolaryngology, Yodogawa Christian's Hospital, Osaka, Japan. From 2001 to 2008, he was an Assistant Professor in Department of Medicine, Graduate School of Medicine, Kyoto University, Japan. Since 2008, he has been a Lecturer in Kyoto University.

Dai Kitagawa received B.S. degree from Department of Mechanical Science and Bioengineering, Osaka University, Japan, in 2007. Since 2007, he has been a master course student in Department of Mechanical Science and Bioengineering, Graduate School of Engineering Science, Osaka University.

Harto Tanujaya received B.S. and M.S. degree from Tarumanagara University, Indonesia and University of Indonesia in 1996 and 1999, respectively. Since 2000, he has been a Lecturer at Department of Mechanical Engineering, Faculty of Engineering, Tarumanagara University. Furthermore, since 2007, he has been a Ph.D. course student in the Department of Mechanical Science and Bioengineering, Graduate School of Engineering Science, Osaka University, Japan.

Satoyuki Kawano received B.S., M.S., and Ph.D. degrees in Mechanical Engineering from Tohoku University, Japan in 1987, 1989 and 1992, respectively. Following graduation he was a Postdoctoral Fellow of the Japan Society for the Promotion of Science in 1992. He was appointed as a Research Assistant in 1993 and as an Associate Professor in 1996 at Tohoku University. In the year of 2005, he was appointed as a Professor at Osaka University where he served as the Chair of the Division of Mechanical Engineering of the Graduate School of Engineering Science from 2006 to 2009. His current research interest is molecular fluid dynamics including interfacial phenomena, plasmas, blood cells and biomacromolecules.

Juichi Ito received M.D. and Ph.D. from Department of Medicine, Kyoto University, Japan, in 1975 and 1983, respectively. From 1983 to 1985, he was an Assistant Professor in Neurology, University of California, Los Angeles. From 1985 to 1990, he was a Lecturer in Department of Otolaryngology Head and Neck Surgery Kyoto University Hospital. From 1990 to 2000, he was a Chief in Otorhinolaryngology and Broncho-Esophagology, Otsu Red-Cross Hospital. Since 2000, he has been a Professor and Chairman of Department of Otolaryngology Head and Neck Surgery, Graduate School of Medicine, Kyoto University.